

Geometric Graph Representation with Learnable Graph Structure and Adaptive AU Constraint for Micro-Expression Recognition

Jinsheng Wei, Wei Peng, Guanming Lu*, Yante Li, Jingjie Yan, and Guoying Zhao, *Fellow, IEEE*

Abstract—Micro-expression recognition (MER) is valuable because the involuntary nature of micro-expressions (MEs) can reveal genuine emotions. Most works recognize MEs by taking RGB videos or images as input. In fact, the activated facial regions in ME images are very small and the subtle motion can be easily submerged in the unrelated information. As a comparison, facial landmarks are a low-dimensional and compact modality, which leads to much lower computational cost and can potentially concentrate more on ME-related features. However, the discriminability of landmarks for MER is not clear. Thus, this paper explores the contribution of facial landmarks and constructs a new framework to efficiently recognize MEs with sole facial landmark information. Specially, we design a separate structure module to separately aggregate the spatial and temporal information in the geometric movement graph based on facial landmarks, and a Geometric Two-Stream Graph Network (GTS-GN) is constructed to aggregate the low-order geometric information and high-order semantic information of facial landmarks. Furthermore, two core components are proposed to enhance features. Specifically, a semantic adjacency matrix can automatically model the relationship between nodes even long-distance nodes in a self-learning fashion; and an Adaptive Action Unit (AAU) loss is introduced to guide the learning process such that the learned features are forced to have a synchronized pattern with facial action units, thus advancing MER. Notably, this work tackles MER only utilizing geometric features, processed based on a graph model, which provides a new idea with much higher efficiency to promote MER. The experimental results demonstrate that the proposed method can achieve competitive or even superior performance with a significantly reduced computational cost, and facial landmarks can significantly contribute to MER and are worth further study for efficient ME analysis.

Index Terms—Micro-Expression Recognition, Facial Landmarks, Graph Network, Action Units.

I. INTRODUCTION

FACIAL expressions can reflect people’s emotions, and representative categories include macro-expressions and micro-expressions. Different from macro-expressions, micro-expressions (MEs) can reflect genuine emotion when people try to hide their emotions. According to the studies [1]–[5] in psychology, MEs are human expressions with rapid, involuntary and low intensity facial movements. Considering that ME can imply the true human emotions and help reveal psychological activities [1], [3], recognizing ME gains increasing attention [6]–[10] and has valuable potential applications, *e.g.* medical diagnosis [5], emotion interfaces [1], security [2], [4], and lie detection [1]–[3].

However, micro-expression recognition (MER), which aims at inferring the category of MEs from ME video clips, is very challenging due to the subtle facial muscle movements and fleeting duration. A lot of works [6], [11]–[17] input RGB images/videos into machine learning models to extract discriminative features, *e.g.*, LBP-TOP with SVM [18], [19] or deep neural networks [8], [12]. Though promising results are achieved, there is still a big space to improve in terms of both accuracy and efficiency. Due to the suppressed property of MEs, only small parts of facial region will be activated in a ME instance. Thus, the computational models will waste huge efforts dealing with redundant information of a whole RGB image/video. Even worse, the ME-related features are prone to be submerged in the irrelevant information thus making MER more difficult. To solve this problem, this paper adopts graph-based model to extract discriminative features only from facial landmarks. In fact, when facial muscle moves, facial landmarks will move accordingly, and thus facial muscle movements in ME can be captured by geometric features in facial landmarks [20]. At the same time, we argue that the extremely compact geometric information is good enough to get comparable even superior performance. Furthermore, time and computational costs regarding landmark-based methods are greatly less than that of image-based methods, which is more desirable for practical applications like in mobile devices. Unfortunately, few works [21] have studied the contribution of geometric features of landmarks for MER tasks. Thus, in this paper, we make the first step to study the discriminability of landmarks and employ only landmarks as input to recognize ME, for exploring its advantages over RGB input.

As we know, the graph-based model can process the facial landmarks lying in the non-Euclidean space. Recently, some works [9], [10], [22], [23] employed the graph-based models to recognize MEs and get promising performance. These works adopt a fixed graph structure that is designed manually according to some principles (*e.g.* the conditional probability of different nodes [22], [24]), namely, the fixed adjacency matrix is defined to represent the fixed relationship between nodes. However, the manual way to set a fixed graph structure is sub-optimal. For overcoming this problem, this paper introduces a learnable adjacency matrix to learn a more reasonable and flexible graph structure based on a pre-defined graph structure. In addition, Action Unit (AU) [25] encodes the local movement of facial muscles and have a strong correlation with MEs. Recently, some works [17], [23] took AU features as input to recognize MEs and used deep

*Corresponding author: Guanming Lu (email: lugm@njupt.edu.cn).

learning models to build the relationship between AU features and ME categories. However, these methods need an auxiliary model to extract AU features before inputting AU features into the main model, which increases the model complexity and computational cost. As there is a close relationship between AUs and the movement of landmarks, thus, different from previous works, our work uses the AU labels as a constraint to make the graph model tend to learn features related to AUs from facial landmarks before the classification layer. In detail, we introduce several multi-label AU losses to constrain the features of different layers in an adaptive way. Furthermore, considering that the contribution of AU losses in different layers is different, this paper proposes an adaptive AU loss to automatically learn the constraint intensity of AU loss in different layers for constraining multi-scale features.

Corresponding to the above problems, the main contributions of this paper can be summarized as follows:

- 1) This work studies the discriminability of facial landmarks for MER and recognizes MEs with the graph-based model by utilizing only geometric features of facial landmarks. The results demonstrate that facial landmarks are discriminative for MER with a largely reduced computational cost. Furthermore, a Geometric Movement Graph (GM-Graph) is first constructed, and a Separate Structure (SS) module is designed to respectively aggregate the spatial and temporal information in GM-Graph. Based on the SS module, a new graph model called Geometric Two-Streams Graph Network (GTS-GN) is introduced to aggregate the low-order and higher-order geometric information of facial landmarks.
- 2) For overcoming the shortcoming of the fixed adjacency matrix in the graph, this paper proposes a Learnable Adjacency Matrix (LAM) to learn a more reasonable and flexible graph structure. As a result, LAM can automatically model the discriminative relationship between facial landmarks for MER.
- 3) Based on the strong correlations of AUs and MEs, the Adaptive AU (AAU) loss is proposed to constrain the features in a multi-scale fashion. AAU loss introduces an automatically learning strategy to emphasize the contributions of features at different semantic levels, and explores a more reasonable way to introduce AU loss. The experimental results demonstrate that AU loss can improve the performance of MER, and AAU loss is superior to the single AU loss that constrains the features of a fixed layer.

II. RELATED WORK

With the research of MER deepen, increasing number of researchers have focused on automatic ME analysis, expecting to explore its value and potential in both academic research and commercial applications. Based on traditional machine learning methods, early works [26], [27] classified MEs using hand-crafted features. These hand-crafted features, *e.g.* LBP-based [7], [13], [26], [28], OF-based [27], [29], [30], HOG-based [31], [32] features, require effort to design, and lacks adaptability. Later, deep learning methods were well applied

in image processing fields, and then some works [33]–[35] in MER began to involve deep learning methods and achieved promising performance. In addition to some classical deep learning models, *e.g.* Convolutional Neural Network (CNN), some recent works [9], [10], [17], [22]–[24] tried to use graph-based models to recognize MEs, and these works have proved the effectiveness of the graph-based methods in MER.

A. Input Datas

So far, many works [7], [26], [28], [34] extract discriminative features from the whole facial RGB images/videos or the feature maps based on these images/videos. However, the extracted features include a lot of redundant information because the discriminative features only exist in a small area of the face, which leads to that the classification model spends too much energy in areas that are not related to MEs, and requires too much computational cost. Although Zong *et al.* [13] proposed the kernelized group sparse learning (KGSL) model to select effective regions, it still requires extracting several hierarchical features from the whole face image, which can improve recognition rate but increase computational cost. To overcome the above problem, Polikovskiy *et al.* [31] divided the Regions of Interest (ROIs) based on the facial landmarks from the whole facial region, and then the features from these ROIs are input into classifier to get ME categories. Some works [31], [36] verified the effectiveness of the features extracted only from ROIs with a reduced computational cost. Furthermore, Liu *et al.* [30] proposed the main direction of optical flow (MDMO) that calculates the main direction of optical flow (OF) in ROIs, thereby the more compact features are input to SVM classifier. Utilizing local regions, instead of the global ones, these works largely reduce the costs. However, these local region-based methods still take up computing resources to first extract the features in the local area, and the computational cost of some features is huge, *e.g.* OF. In addition, region cropping is also a not trivial issues.

In MER, facial landmarks need to be extracted for face alignment, interception, and the division of regions, especially the division of local regions in local region-based methods, thereby extracting facial landmarks is unavoidable. At the same time, when facial muscle moves, facial landmarks will move accordingly, and thereby facial muscle movements in ME can be captured by the geometric features in facial landmarks. Therefore, we argue that geometric information is discriminative enough to get comparable even superior performance, and it may not be necessary to perform complicated and costly pre-processing from the raw RGB inputs. Compared with images/videos, the low dimensional landmarks are much more compact, as well can include the discriminative geometric feature information [37]. Choi *et al.* [21] employed facial landmarks as the input to recognize MEs instead of original ME images/videos. Specifically, they proposed 2D landmark feature map (LFM) by transforming conventional coordinate-based landmark information into 2D image information and employed CNN and Long Short Term Memory (LSTM) models to process it. The work aggregated feature information in facial landmarks and got promising results, but

the model input still is the 2D image. Recently, Kumar *et al.* [10] proposed a two-stream Graph Convolutional Network (GCN) [38] model, and one of the streams deals with landmarks. However, they do not focus on landmarks or explore their discriminability and efficiency, and optical flow features also need to be extracted as inputs. This paper focuses on the effectiveness of facial landmarks in terms of both accuracy and efficiency and explores more effective module to aggregate spatial and temporal information in facial landmarks. Since the landmarks are structure data lying in the Non-Euclidean space, a new graph model is designed to learn the geometric feature representations of MEs from the facial landmarks.

B. Graph Models

Recently, graph-based methods are popular in MER and generally don't input the whole facial images into models. According to the way to construct graph, these methods can be divided into two types: landmark-based and AU-based.

Lei *et al.* [9] firstly constructed a landmarks based graph, and the magnified shape features around landmarks were taken as node features, but they ignore the special relationships of nodes and only employed Temporal Convolutional Network (TCN) [39] to deal with the node representation. Recently, Kumar *et al.* [10] took the facial landmarks and optical flow features around landmarks as node features and designed Graph Attention Convolutional Network (GACN) to process the landmark-based graph. Except for facial landmarks, AU also is suitable to construct the graph. Lo *et al.* [24] designed GCN with two layers to deal with AU-based graph and aggregate AU label information that dots product with spatial-temporal features extracted by 3D convolution. They explore the relationship between AUs and MEs, but the node features are the annotated AU labels, which is not suitable for practical applications. Furthermore, both [17] and [23] took the AU features extracted by extra model as node features in AU-based graph. Differently, Zhou *et al.* [17] connected the inception block and an AU detection module to extract AU features, while Xie *et al.* [23] employed 3D ConvNet to extract AU features. Lei *et al.* [22] introduce transformer and AU features to extend their previous work [9] through combining two types of graph. However, on one hand, the existing works with landmark-based graph aggregated dynamic information, *e.g.* optical flow and magnified shape feature, which still spends too much computational cost to extract these features; on the other hand, the works with AU-based graph need extra learning model to extract AU features as node feature, which increases the model complexity and computational cost, and AU detection for MER itself is a very challenging task. Inspired from skeleton-based action recognition works, *e.g.* [40], instead of providing much complicated and costly appearance features or not easily accessible AU features, we provide a simple and much efficient way that directly takes landmark coordinate-based geometric features as node features and employs graph models to deal with such geometric features for MER. Furthermore, the proposed module employs GCN and TCN to aggregate spatial and temporal information in the geometric movement graph, respectively, and a new graph

network is designed to aggregate the low and high order geometric information from facial landmarks. Furthermore, this work also involves the relationship between nodes in graph and the AU information. The related works are as follows:

The Relationship between Nodes: The relationship between nodes is key to aggregate the feature information in graph and can be expressed as the adjacency matrix. Although Lei *et al.* [9] defined a graph, they didn't give the adjacency matrix in the graph, namely, the special relationship between nodes do not be considered. Most of the above graph-based methods built the relationship between nodes according to some principles. Specifically, based on the human facial structure, Kumar *et al.* [10] built the relationship between landmark nodes; [23] first connected AU nodes based on the AU correlations of the objective class definition and then adjusted it referring to the training datasets; [17] achieved it by the training set based on common facial expressions and facial anatomy analysis; [22] and [24] defined adjacency matrix by a data-driven way, and both use the conditional probability of different nodes. Different from these methods, we first pre-defined a fix adjacency matrix based on facial muscle structure, and then, we define a LAM that are added to the fix adjacency matrix and learn more reasonable relationship between nodes.

AU Information: As we know, AUs have the closed relation with facial expressions, including MEs. At present, AU recognition received widespread attention, and the researchers in MER have introduced AU information to recognize MEs. In [24] and [22], AUs are fed into the GCN model to learn the AU representations, and the learned AU representations are fused with ME representations extracted by other models. However, the two methods need to compute the AU vector in advance. [23] and [17] introduced AU loss to extracted AU representation from original video data or optical flow map, and then, the learned representations are aggregated by GCN for final classification. These methods need the extra models to process AUs or learn AU representation, which increases the model complexity and computational cost. Different from these works, we propose an AAU loss to aggregate AU information and constraint the features in a multi-scale fashion without extra models. In AAU loss, the learnable weights for multiple AU losses emphasize the contributions of features at different semantic levels, and thereby, AAU loss can constraint the multi-scale features in an adaptive way.

III. THE PROPOSED METHOD

In this section, the proposed method will be introduced in detail, and we present the framework of the proposed graph model as shown in Fig. 1. This work constructs a GM-Graph, designs SS module to deal with GM-Graph, and builds the GTS-GN model. Furthermore, two components (LAM and AAU loss) are proposed to enhance the ME features. The subsections include four parts: GM-Graph, SS module with LAM, GTS-GN, and AAU loss. The details are as follows.

A. Geometric Movement Graph

Considering the subtle movement in MEs, the extraction of movement features is crucial to MER tasks. The onset,

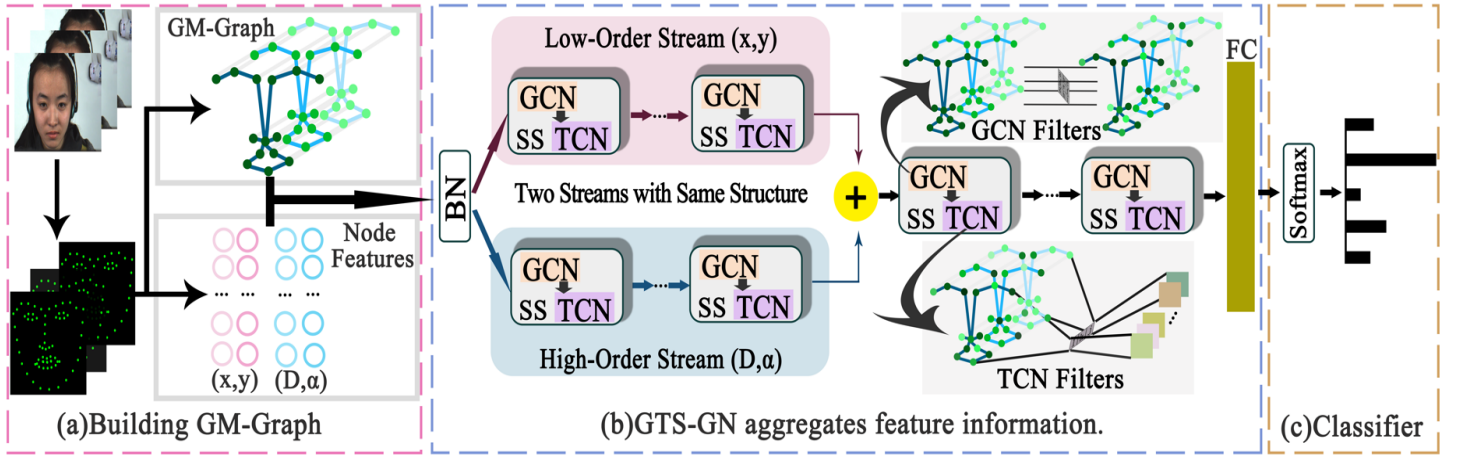


Fig. 1. The flowchart of GTS-GN. GTS-GN aggregates the geometric information of low order coordinate (x, y) and high order semantic (D, α) .

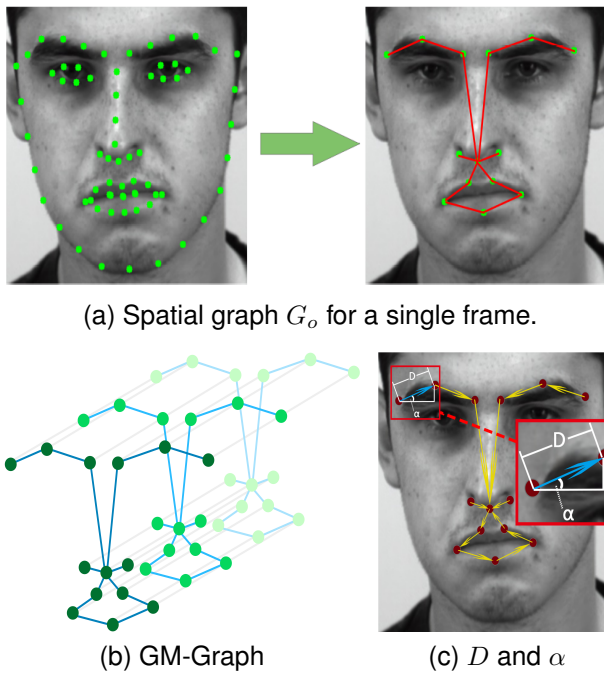


Fig. 2. The construction of GM-Graph based on onset, apex, and offset frames, and the calculation of the distance D and angle α .

apex and offset frames represent the key process of muscle movement when MEs occur, thus these three frames contain abundant movement information and remove a lot of redundant frames in the entire video. As in the existing works of MER, *e.g.* [6], [9], these three frames can be found based on labels on databases, and their detection belongs to another task [14], [41], [42] in ME analysis. Based on these three frames, a spatial-temporal graph GM-Graph is constructed for MER. The detection of landmarks is necessary for aligning face in the movement features-based methods, and the facial landmarks of the onset, apex and offset frames include the discriminative movement information. Thus, in this paper, the landmarks of the onset, apex and offset frames in ME videos are taken as nodes in GM-Graph to capture the ME movements as shown in Fig. 2. Furthermore, inspired by the Facial Action Coding System (FACS) [25], we choose the landmarks around the mouth, eyebrows and nose to construct the graph based on

their contributions. Here, the landmarks in the eye region don't be considered, and the reasons are as follows: 1) some noises in the eye regions are exist, *e.g.* blink; 2) the change in the eye regions about MEs can lead to the corresponding change in eyebrows, *e.g.* dilation of pupils in a surprised expression, and there is some redundant information.

As shown in Fig. 2a, we select 14 key points as the nodes of the spatial graph from facial landmarks. Considering the natural connection of the facial regions, we build the spatial relationship between landmarks for a single frame and construct the landmark-based spatial graph $G_o = \{N_o, E_o\}$, where N_o and E_o are the node set and edge set in spatial graph, respectively. Furthermore, movement features need to be extracted from temporal information that is key to recognize MEs. Thus, based on the G_o of the onset, apex and offset frames, the GM-Graph G_{GM} is constructed to establish the spatial-temporal relationship between landmarks. As shown in Fig. 2b, for modeling temporal information, the corresponding nodes between three frames also are connected. Thus, GM-Graph $G_{GM} = \{N, E\}$ is constructed, where N and E are the node set and edge set in GM-Graph, respectively, N is a collection of the N_o of three frames, and E denotes the connection of nodes in GM-Graph.

The node feature is crucial to represent the spatial-temporal information. In fact, the facial muscles move when MEs appear, which leads to the movement of landmarks. Thus, the landmark coordinates include the movement information of MEs. Also, the data dimension of landmark coordinates is much smaller than that of the raw frames, which is more efficient and can save computational resources to facilitate practical applications. In this paper, only landmark coordinates $n = (x, y)$ are adopted as nodes features to study the effectiveness of landmarks, and higher-order semantic features (distance and angle between landmarks) are added to explore the interaction of low and high-order geometric information.

Fig. 2c shows the calculation of distance D and angle α based on landmark coordinates. Suppose that $n_i = (x_i, y_i)$ (the start point of the arrow in Fig. 2c) is the current node, and $n_j = (x_j, y_j)$ (the end point of the arrow) is the neighboring

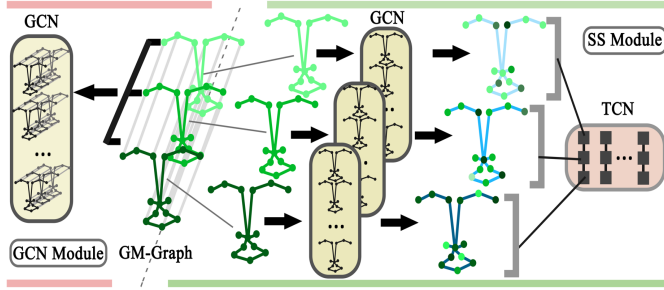


Fig. 3. The comparison of GCN and SS Modules.

node. D and α can be calculated by:

$$\begin{cases} D = (x_i - x_j)^2 + (y_i - y_j)^2 \\ \alpha = \arctan((y_i - y_j)/(x_i - x_j)) \end{cases} \quad (1)$$

where $\arctan(*)$ is the arctangent function.

According to the description above, we define two types of node features that (x, y) is Type A, and (x, y, D, α) is Type B, where (x, y) is the landmark coordinates.

B. SS Module

Inspired by CNN+LSTM [21] that extracts spatial-temporal features separately, we design SS module to aggregate spatial and temporal information in GM-Graph. The movement of the landmarks in ME is small, and the movement of each node along the time step is key to recognize MEs. Thus, the extraction of temporal features is crucial and challenge for MER. GCN can simultaneously extract the spatial and temporal features in the spatial-temporal graph, but cannot focus on the extraction for the temporal features, which maybe neglect some small movement features. Thus, in this paper, TCN is adopted to focus on temporal information in GM-Graph. Furthermore, considering that the spatial features of each frame also includes important information, *e.g.* geometric and structure information, GCN is employed to aggregate spatial information in GM-Graph. As shown in Fig. 3, SS module adopts GCN to aggregate the spatial information for three frames, respectively, and then, TCN is adopted to aggregate the temporal information between three frames. Like that, every operation focuses on the aggregation of one type of information (spatial or temporal), which facilitates learning finely more discriminative features.

GCN with the Learnable Adjacency Matrix: Specifically, SS module first splits GM-Graph into three sub-graphs $\{G_{GM^1}, G_{GM^2}, G_{GM^3}\}$ that correspond to the spatial graph G_o of three frames. Suppose that A is the pre-defined adjacency matrix that expresses the node connection in G_o , and $A \in \mathbb{R}^{14 \times 14}$. By normalizing A , we can get $L = I_n - D^{-1/2}AD^{-1/2}$, where $D = \sum_j A_{ij}$ is the degree matrix. Then, L is used for Fourier transform, and for G_{GM^f} ($f = 1, 2, 3$) with spatial information, the graph is filtered by g_ϕ to get the output node features Y^f as follows:

$$Y^f = g_\phi(L)X = Ug_\phi(\Lambda)U^T X^f, \quad (2)$$

where X^f is the node features of G_{GM^f} ; U is the Fourier basis and a set of orthonormal eigenvectors for L ; and $L = U\Lambda U^T$

with Λ as corresponding eigenvalues. Considering the calculation of eigenvectors matrix is expensive, so a Chebyshev polynomial with R -th order is employed to well-approximate the filter g_ϕ as follows:

$$Y^f = \sum_{r=1}^R \theta_r C_r(\hat{L})X^f \quad (3)$$

where θ_r denotes Chebyshev coefficients, and $C_r(\hat{L})$ denotes Chebyshev polynomial. $\hat{L} = 2L/\lambda_{max} - I_n$ is normalized to $[-1, 1]$, and $C_r(\hat{L}) = 2\hat{L}C_{r-1}(\hat{L}) - C_{r-2}(\hat{L})$, where $C_0 = 1$ and $C_1 = \hat{L}$. Suggested by [38], $R = 1$, and $\lambda_{max} = 2$. Then,

$$\begin{aligned} Y^f &= \theta_0 X^f - \theta_1 (D^{-1/2}AD^{-1/2})X^f \\ &= \theta(I_n + D^{-1/2}AD^{-1/2})X^f \end{aligned} \quad (4)$$

where θ_r is approximated to a unified θ , and $\theta = \theta_0 = -\theta_1$. Finally, for simplifying expression, we set $L = I_n + D^{-1/2}AD^{-1/2}$ and the final form of GCN is:

$$Y^f = GCN(G_{GM^f}) = LX^f\theta \quad (5)$$

where θ is the learnable filter.

Learnable Adjacency Matrix LAM: The above pre-defined adjacency matrix A is fixed and expresses a fixed relationship between nodes. Furthermore, the fixed relationship is defined according to some principles (*e.g.* facial structure [10] and data-driven [22], [24]) set by the researchers and is sub-optimal. Thus, we introduce LAM expressed as A_L to learn a more reasonable relationship between nodes. Considering that the fixed A has certain rationality, A is retained. Therefore, the final form of GCN with LAM is as follows:

$$Y^f = GCN'(G_{GM^f}) = (L + A_L)X^f\theta \quad (6)$$

where A_L can be updated and learned automatically in the training stage of model.

TCN: After getting the spatial graph representation processed by GCN with LAM, TCN is employed to extract temporal features between $\{G_{GM^1}, G_{GM^2}, G_{GM^3}\}$. so the temporal feature F_n^T of n -th node is:

$$F_n^T = TCN(Y_n^1, Y_n^2, Y_n^3) = Y_n W \quad (7)$$

where $Y_n = [Y_n^1, Y_n^2, Y_n^3]$, and W is the learnable filter. Thus, SS module can be formed by:

$$TCN(GCN'(G_{GM^1}), GCN'(G_{GM^2}), GCN'(G_{GM^3})) \quad (8)$$

As basic blocks, several SS modules are stacked directly to build SS Graph Network (SS-GN). Also, based on SS modules, GTS-GN is built as follows.

C. Geometric Two-Stream Graph Network

Besides the low-order coordinates, the geometric features also include the high-order semantic features, *e.g.* distance D and angle α above. The distance and angle of landmarks include semantic information and can provide more discriminative features to improve performance. However, it is difficult

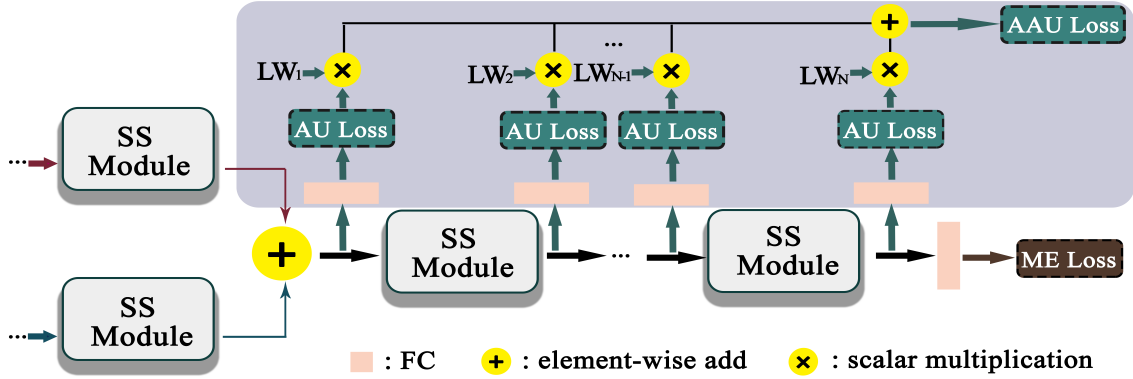


Fig. 4. The calculation of the total loss. In this figure, LW_r and N are $\frac{W_r^2 L_r}{\sum_{r=1}^{N_L} W_r^2}$ and N_L , respectively.

to learn the discriminative features from the information interaction of the low-order and high-order representations since the two features have different distributions. Also, training two models to deal with two features separately cannot take into account the interaction of the two features, and the model is not end-to-end. Thus, an end-to-end model that is able to aggregate low-order and high-order features separately is needed. We propose a new graph model called GTS-GN to process low-order and high-order geometric features in two streams. Both features processed by GTS-GN belong to geometric features, and there is a certain correlation between the two features. Thus, different from the existing two-stream models that fuse two features in last layer, *e.g.* [10], GTS-GN tries to fuse the two features at the earlier layer, not limited to the last layer. The whole network is shown in Fig. 1.

Specifically, the low-order coordinates and high-order semantic features have some differences in feature distribution, so we employ Batch Normalization (BN) to normalize the two features. Next, two types of features are inputted into two streams, and two streams adopt the same structure that stacks several SS modules with the same number. After several SS modules, the outputs of two streams are added together, and the added features are inputted into several SS modules or Full Connected (FC) layer to continue aggregate geometric feature information. Finally, the softmax is used to classify features and predict the ME categories.

D. Adaptive AU Loss

As we know, the correlation between AU and ME is strong, and using the strong correlation is beneficial to recognize MEs [23]. Thus, our model builds this correlation by learning the features related to AU before the ME classification layer, thereby improving MER. In this paper, loss function are employed to achieve this intention by constraining feature way.

For AU recognition, the multi-label AU loss is used to constrain the learned features to make them relevant to AU for recognizing AU categories. Differently, our aim is to constrain the learned features to make them relevant to AU for recognizing ME categories. Thus, we introduce multi-label AU loss before ME classification layer, instead of at classification layer. Furthermore, the multi-scale features in multiple layers are constrained by the proposed AAU loss as shown in Fig. 4. In order to better aggregate low-order

and high-order information individually before fusion, AAU loss constrains the features after fusing the two streams. Now, supposed that the features of N_L layers are constrained, and the corresponding multi-label AU loss is L_r ($r = 2, \dots, N_L$), so, the loss to constrain the multi-scale features is as follows:

$$L' = \sum_{r=1}^{N_L} L_r \quad (9)$$

where L_r is conducted by *MultiLabelSoftMarginLoss* package in Pytorch [43]. However, there is a shortcoming in Equation 9, that is the constraint strengths in all layers are the same, which can't consider the difference between the features of different scales. Thus, we introduce the learnable weights to these losses for emphasizing the contributions of features at different semantic levels as follows:

$$L'' = \sum_{r=1}^{N_L} W_r L_r \quad (10)$$

where W_r is learnable weight and can be updated in training stage. In fact, Equation 10 make the model tend to learn the W_r s with all zero values. Furthermore, the positive weights also is needed. Thus, to overcome the two problems, we take probability form as the weight to get AAU Loss as follows:

$$L_{AAU} = \sum_{r=1}^{N_L} \frac{W_r^2 L_r}{\sum_{r=1}^{N_L} W_r^2} \quad (11)$$

where $N_L \geq 2$ due to the AAU loss will degenerates to AU loss when $N_L = 1$.

Total Loss: The task for this work is MER. Thus, ME labels are employed to calculate cross-entropy loss as ME loss (L_{ME}) in the final classifier. Thus, the total loss (L_T) is as follows:

$$L_T = L_{ME} + \beta * L_{AAU} \quad (12)$$

where β is the trade-off parameter.

IV. EXPERIMENTS

This section reports the experimental results that study the effectiveness of landmarks and evaluate the performance of the proposed method. First, the effectiveness of facial landmarks

TABLE I
THE CATEGORIES OF THE USED SAMPLES.

| Based on AUs | | | | | | | |
|--------------|---|----|-----|----|---|----|-----|
| Type | I | II | III | IV | V | VI | VII |
| ① | ✓ | ✓ | ✓ | ✓ | ✓ | | ✓ |
| ② | ✓ | ✓ | ✓ | ✓ | ✓ | | |

| Based on self-report | | | | | | | |
|----------------------|-------|---------|------------|----------|-----|------|--------|
| Type | happy | Disgust | Repression | Surprise | Sad | Fear | Others |
| ③ | ✓ | ✓ | ✓ | ✓ | | | ✓ |

(a) On CAMSE II

| Based on AUs | | | | | | | |
|--------------|---|----|-----|----|---|----|-----|
| Type | I | II | III | IV | V | VI | VII |
| ① | ✓ | ✓ | ✓ | | ✓ | | ✓ |
| ② | ✓ | ✓ | | ✓ | ✓ | | |

| Based on self-report | | | | | | | | |
|----------------------|-------|---------|-------|----------|-----|------|----------|--------|
| Type | happy | Disgust | anger | Surprise | Sad | Fear | contempt | Others |
| ③ | ✓ | | ✓ | ✓ | | | ✓ | ✓ |

(b) On SAMM

TABLE II
THE FEATURE DIMENSION OF EVERY LAYER IN ALL GRAPH MODELS USED IN OUR EXPERIMENT. C IS THE NUMBER OF CATEGORIES.

| layer | 1 | 2 | 3 | 4 | FC |
|------------------|--------|----|-----|-----|-----|
| Input dimension | 2 or 4 | 64 | 64 | 128 | 128 |
| Output dimension | 64 | 64 | 128 | 128 | c |

is studied for MER; Second, we carry out ablation analysis with some visualizations to evaluate the proposed components, including SS module, GTS-GN, LAM, and AAU loss; Third, the parameter evaluation is carried out; Finally, we compare the proposed method with state-of-the-art (SOTA) methods.

A. Experimental Setting

The experiments are carried out on SAMM [44] and CASME II [45] datasets. In CASME II, all participants are from one ethnicity, and it contains 255 video samples from 26 subjects with seven ME categories based on self-report; In SAMM, participants are from 13 ethnicities, and it includes 159 samples from 32 subjects with eight ME categories based on self-report; For the same points, the video samples in both datasets are collected by the high-speed cameras at 200 fps, and both datasets contain AU annotations that can form seven ME categories based on AU annotations;

In this work, the ME categories based on AU annotations are adopted to evaluate the proposed method. Like in previous MER tasks [7], [14], due to the long-tail distribution of the samples, we deleted the categories with less than ten samples. As a result, six and four ME categories based on AU annotations (Type ① in Table I) are selected from CASME II and SAMM, respectively. Furthermore, the existing methods in MER used not only AU annotations, but also self-reported annotations. Thus, for a more comprehensive and fair comparison with SOTA methods, we show the results of the proposed method on other two types of category setting: under five ME categories based on AU annotations (Type ② in Table I) following [46] and under five ME categories based on self-report (Type ③ in Table I) following [10].

In our experiments, the facial muscle movements are magnified by a learning-based motion magnification method [47], such that the movements of landmarks are more obvious.

TABLE III
COMPARISON OF RESNET18, CAPSULE, GCN AND SS-GN. ACC(%).

| Methods | CAMSE II | | SAMM | |
|--------------|--------------|--------------|--------------|--------------|
| | ACC | F1 | ACC | F1 |
| ResNet18 [8] | 66.13 | 0.588 | 68.57 | 0.649 |
| Capsule [8] | 66.53 | 0.612 | 64.54 | 0.587 |
| GCN [38] | 70.12 | 0.690 | 70.21 | 0.661 |
| SS-GN | 72.90 | 0.716 | 75.17 | 0.732 |

(a) The comparison performance.

| Methods | Input size | Average Time | Parameter |
|--------------|------------|--------------|------------|
| ResNet18 [8] | 3*224*224 | 0.0087 | 11,179,590 |
| Capsule [8] | 3*224*224 | 0.0216 | 14,284,864 |
| GCN [38] | 42*2 | 0.0038 | 39,760 |
| SS-GN | 14*3*2 | 0.0050 | 163,710 |

(b) The costs. Average Time (Unit: sec.)

The amplification factor is set to three following the setup in [9]. Then, the Dlib [48] package is employed to detect facial landmarks. To study the effectiveness of landmarks, the basic graph-based models with landmark are compared to the basic CNN and Capsule model with image: ResNet18 and Capsule [8]. All graph-based models used in our experiment have four layers, and the feature dimensions in different layers are shown in Table II. β is set to [0.1,1] with interval 0.1 in parameter evaluation and is fixed to 1 in the ablation study. To explore a better way to fuse the features from the two-stream inputs, GTS-GN is implemented in four types according to in which layer the two streams are merged, namely GTS-GN (layer n), $n = 1, 2, 3, 4$. The filter size of TCN is three to cover the node features in three frames. For all experiments, two evaluation matrices under leave-one-subject-out (LOSO) strategy are adopted to evaluate different methods, including accuracy(ACC) and F1-score.

Data augmentation is important for the training of the deep models. In our experiments, the ResNet18 and Capsule take the magnified apex frame as input and augment the data by rotation, adding noise, cropping randomly, horizontal flip and color jitter. Also, considering the detected landmarks for the face regions with different sizes have a small difference, we can regard this difference as noise to extend data. The aligned frames are cropped to get the frames of different sizes, and then we detect the landmarks of these frames with different sizes to obtain more data. All models are trained on a single GTX 1050 GPU with Pytorch [43] deep learning framework.

B. The Study on the Effectiveness of Landmarks

First of all, we evaluate the effectiveness of landmarks compared with images in terms of recognition performance and model efficiency. For fair comparison, we use vanilla models to process images and landmarks. In terms of image-based models, basic CNN and Capsule models are adopted to process apex frame that is Euclidean data, and correspondingly, basic graph models are adopted to process the landmark that is Non-Euclidean data. Specifically, image-based ResNet18 and Capsule are compared with landmark-based GCN and SS-GCN. As shown in Table III(a), comparing with image-based ResNet18 and Capsule, landmark-based GCN and SS-GCN get substantially better performance under both evaluation

TABLE IV
THE EVALUATION ON SS MODULE AND GTS-GN. ACC(%).

| Methods | CAMSE II | | SAMM | |
|---------------|--------------|--------------|--------------|--------------|
| | ACC | F1 | ACC | F1 |
| GCN+Type A | 70.12 | 0.690 | 70.21 | 0.661 |
| SS-GN+Type A | 72.91 | 0.716 | 75.17 | 0.732 |
| SS-GN+Type B | 72.91 | 0.710 | 73.05 | 0.693 |
| GTS-GN+Type B | 73.31 | 0.717 | 75.89 | 0.741 |

(a) Graph models with different node features.

| Methods | CAMSE II | | SAMM | |
|------------------|--------------|--------------|--------------|--------------|
| | ACC | F1 | ACC | F1 |
| GTS-GN (layer 1) | 73.31 | 0.717 | 76.60 | 0.729 |
| GTS-GN (layer 2) | 72.91 | 0.714 | 75.17 | 0.723 |
| GTS-GN (layer 3) | 71.71 | 0.690 | 73.05 | 0.708 |
| GTS-GN (layer 4) | 68.13 | 0.640 | 75.89 | 0.741 |

(b) GTS-GN (n layer), n = 1, 2, 3, 4.

metrics. For instance, SS-GCN improves the ACC by 6.37% and 10.63%, compared with Capsule, on CASME II and SAMM, respectively. It demonstrates that facial landmarks is discriminative for MER. For the model efficiency, as shown in Table III(b), our SS-GCN can be about 1.7 and 4.3 times faster than image-based ResNet18 and Capsule, respectively. In particular, the model size of SS-GCN is about only 1.5% and 1.1% of that of ResNet18 and Capsule, which is essential to real-time applications. In addition, landmark-based GCN and SS-GCN have an obvious advantage on input dimension.

To summarize, the results above demonstrate that the movement of landmarks contain the discriminative features and can be effectively used to recognize MEs. The below experiment (the results comparing with other methods are as shown in Tables X and XI) can also demonstrate the discriminability of landmarks for MER tasks. Also, the geometric features in landmarks are more compact representations with a largely reduced computational cost. Overall, the landmark-based graph models have much higher computational and parameter efficiency than the image-based models for MER tasks.

Discussions: Notably, our method is based on landmarks, so the accuracy of detecting landmarks is key for our method. In fact, if the detected landmarks have a huge error, the methods that need to use landmarks will be significantly affected. On one hand, in MER task, all existing movement-based methods need to detect landmarks to align faces, and the crop of local areas in the local feature-based methods [10], [22], [30], [39] also depends on landmarks, so this problem is inevitable in MER task; on the other hand, for the used datasets, the scenarios are controlled and rather simple, so landmarks can be reliably detected. But when moving to uncontrolled environment with complicated mixed movement and big illumination changes, more powerful landmark detection technology is needed for getting accurate landmarks. Fortunately, the detection technologies of landmarks are ongoing research, and some works [49] have promising results, which is technical support for landmark-based methods. In addition, image-based methods also are greatly affected in complex environments, thus, MER under complex environments is another unsolved and challenging task.

Overall, the landmark-based methods face the above-

mentioned inevitable problems like other image-based methods. Although image-based methods can aggregate more appearance information, the landmark-based methods can avoid the cumulative error caused by cropping the ROI areas and extracting features in these areas. In addition, this paper demonstrates the discriminability and efficiency of landmarks, yet the geometric features from landmarks and the appearance features from ME images do not conflict. Therefore, how to better combine the appearance features with the geometric features is also worthy of further study.

C. Ablation Analysis

This section shows and analyzes the results of ablation study for the proposed components and can be divided into three sub-sections: the evaluation on SS-module and GTS-GN, the evaluation on LAM, and the evaluation on AAU Loss.

1) *The Evaluation on SS-module and GTS-GN:* **The Evaluation on SS-module:** We evaluate SS module, and the vanilla GCN [38] is taken as baseline and directly processes the whole GM-Graph. As shown in Table IV(a), taking landmark coordinates (Type A) as node features, SS-GN outperforms GCN in terms of both accuracy and F1-score for both datasets, which demonstrates that the features extracted by SS module are more discriminative than those extracted by GCN, and extracting spatial and temporal geometric features separately is a better choice for MER.

The Evaluation on GTS-GN: We evaluate the performance of GTS-GN which aggregates low-order and high-order geometric features, *i.e.*, Type B (x, y, D, α) is taken as node features. According to Table IV(a), SS-GN+Type A is superior to SS-GN+Type B, which proves that simply introducing high-order geometric information cannot ensure performance improvement. Furthermore, GTS-GN+Type B outperforms both SS-GN+Type B and SS-GN+Type A, which demonstrates that GTS-GN can aggregate the low-order and high-order geometric information more effectively than SS-GN, and distance D and angle α provide the discriminative high-order geometric information to recognize MEs. In addition, we explore a better way to fuse two feature flows in GTS-GN. As listed in Table IV(b), interestingly, we find that different datasets prefer different ways to fuse the features. For CASME II, fusing the two-stream features at layer one provides better performance, while for SAMM, fusing at fourth layer provides a better F1-score and a comparable accuracy. This may be caused by the different ME categories in these two datasets. The experiment results prove that the fusing two feature flows in the last layer is not optimal, and earlier fusion may result in better performance.

Overall, SS module can effectively aggregate spatial-temporal information in GM-Graph, and the GM-Graph with only geometric features as node features can be processed by graph model to get promising results. Also, GTS-GN provides flexibility to fuse and aggregate the low-order and high-order geometric features, which is more effective than one stream-based SS-GN.

2) *The Evaluation on Learnable Adjacency Matrix:* To evaluate the effectiveness of LAM, the GTS-GN with LAM

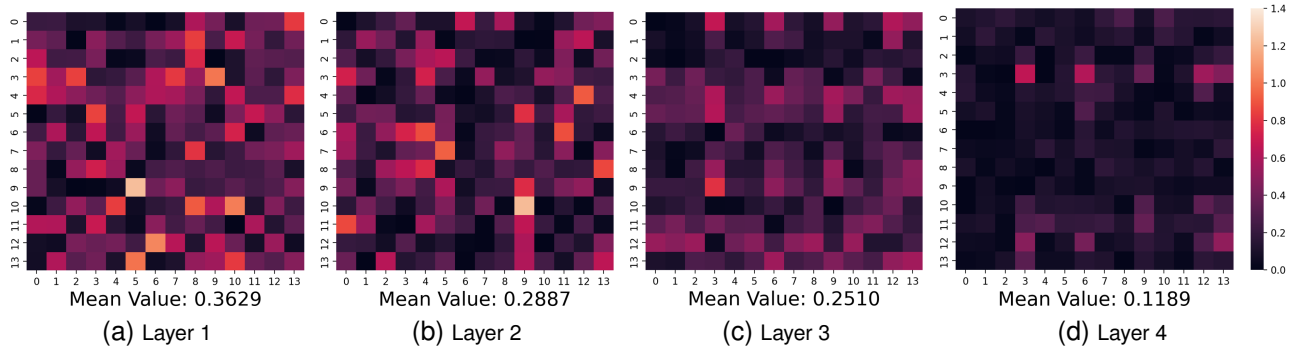


Fig. 5. The visualization results of LAM. (a) to (d) mean the LAMs in layers 1 to 4, respectively.

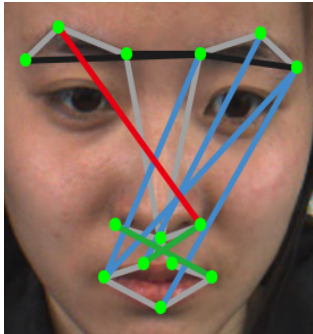


Fig. 6. The visualization for LAM in layer 1. The line connecting two nodes indicates that the two nodes are strongly correlated, namely, the value in LAM is more larger. Red line: eyebrows-nose; Blue line: eyebrows-mouth; Green line: nose-mouth; Black line: eyebrows, where A-B indicates that the connects are between A and B regions.

are compared with GTS-GN without LAM. Table V shows the results. It turns out that both GTS-GN without and with AAU loss are improved after adding LAM, which proves that LAM is effective for MER to learn more reasonable adjacency matrix, namely, LAM is superior to a fixed adjacency matrix.

Visualization: In order to illustrate the advantages of LAM intuitively, we visualize the learned LAM on CASME II. Fig. 5 shows the heatmap of the learned LAMs in different layers. From this figure, the different layers have different LAMs, and as the layer increases, the average value of the learned LAM is smaller. It can be interpreted as that the node features in earlier layers represent low-level feature information, and the relationship between different nodes is strong to be aggregated to high-level feature information. Thus, in earlier layers, the relationship between different node features is modeled using an adjacency matrix with larger values. For the deeper layers, every node feature represents higher-level information and already interacts with other node features, and the correlation between nodes weaken, thus an adjacency matrix with smaller values is enough to model the relationship between node features. Furthermore, we visualize the ten edges with larger values in the LAM of the last layer. As shown in Fig. 6, LAM can learn the relationship between different facial muscle regions that do not have connections in the pre-defined adjacency matrix, e.g. the relationship between the nodes feature of mouth and eyebrows regions, which makes that the model can aggregate the node features more effectively.

Overall, LAM can consider the difference of different layers to build the relationship between different facial organs in multi-scales, thereby, more reasonable adjacency matrices can

TABLE V
THE ABLATION STUDY ON LAM AND AAU LOSS. ACC(%).

| Components | | | CAMSE II | | SAMM | |
|------------|-----|----------|--------------|--------------|--------------|--------------|
| GTS-GN | LAM | AAU Loss | ACC | F1 | ACC | F1 |
| ✓ | × | × | 73.31 | 0.717 | 75.89 | 0.741 |
| ✓ | ✓ | × | 74.90 | 0.732 | 78.01 | 0.782 |
| ✓ | × | ✓ | 76.10 | 0.745 | 78.01 | 0.756 |
| ✓ | ✓ | ✓ | 77.29 | 0.765 | 79.43 | 0.782 |

TABLE VI
THE EVALUATION ON GTS-GN WITH AU LOSS. AU LOSS N DENOTES THAT AU LOSS CONSTRAIN THE FEATURES IN THE N-TH LAYER. ACC(%).

| Methods | CAMSE II | | SAMM | |
|-----------------------|----------|-------|-------|-------|
| | ACC | F1 | ACC | F1 |
| GTS-GN | 72.91 | 0.697 | 70.92 | 0.673 |
| GTS-GN with AU loss 1 | 73.31 | 0.712 | 75.18 | 0.743 |
| GTS-GN with AU loss 2 | 71.71 | 0.697 | 74.47 | 0.713 |
| GTS-GN with AU loss 3 | 73.31 | 0.727 | 75.18 | 0.729 |
| GTS-GN with AU loss 4 | 72.91 | 0.708 | 75.18 | 0.724 |

be learned to aggregate the node features.

3) *The Evaluation on Adaptive AU Loss:* In this section, we show the results of GTS-GN, GTS-GN with AU loss and AAU loss, and evaluate AAU loss in detail by visualization.

First of all, we evaluate the AU loss in details. GTS-GN (layer 1) is taken as an example because it includes more constrained layers ($N_L = 4$). Table VI shows the results that add AU loss to 4 layers, respectively. It turns out that constraining the features in different layers has different performance, and overall, the performance is improved after using AU loss. In addition, the performance maybe worse after adding AU loss in some layers, e.g. layer 2 on CASME II.

Next, AAU loss is effective and can improve the performance as shown in Table V. From Table V, both GTS-GN and GTS-GN with LAM achieve a better performance after adding AAU loss, which demonstrates that AAU loss is helpful to extract more discriminative features for recognizing MEs.

Furthermore, as shown in Table VII, AAU loss is compared with AU loss and basic model (GTS-GN) under four types of GTS-GN, where GTS-GN (layer 4) with AAU loss don't have results because the constrained layer in GTS-GN (layer 4) only has one while $N_T > 1$. Overall, according to this table, AAU loss can achieve the best performance for every type of GTS-GN, and AU loss can improve GTS-GN in most cases. Compared with GTS-GN, AAU loss can greatly improve the performance in all cases; on the other hand, although AU loss doesn't promote GTS-GN (layer 2) on SAMM, it

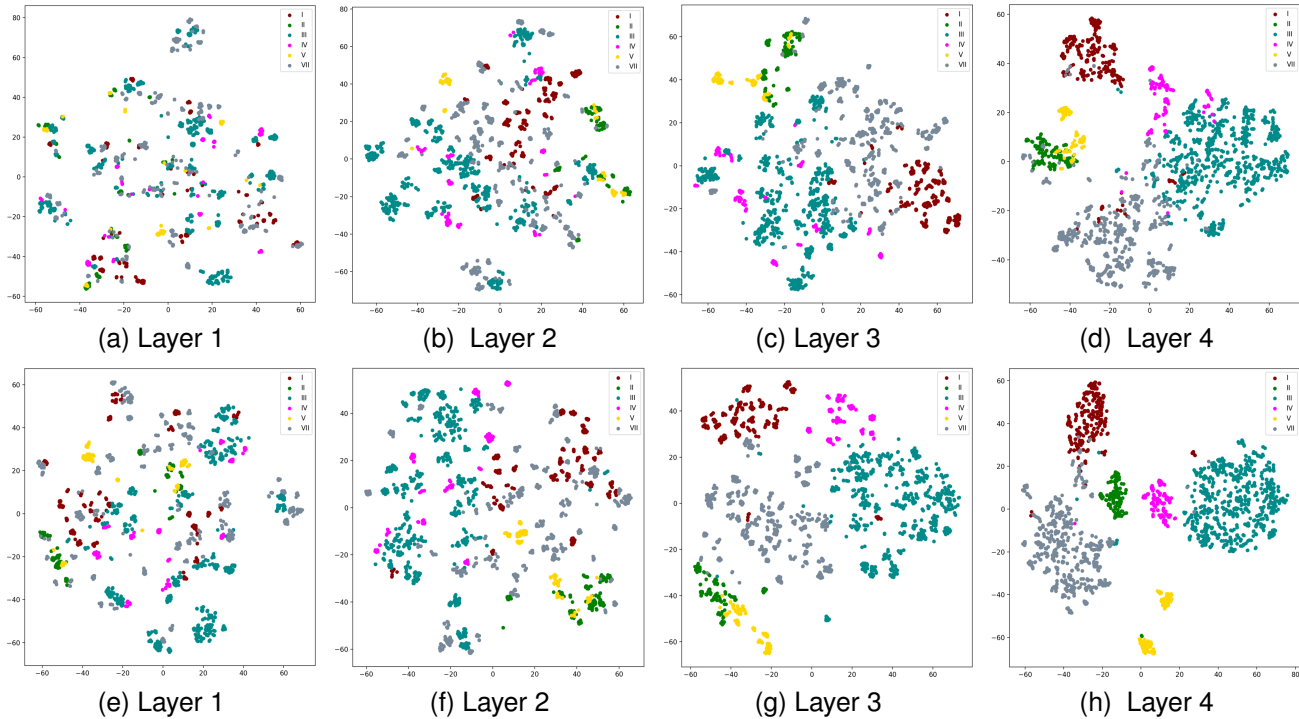


Fig. 7. The visualization of the features in different layers using t-SNE. The first and second rows are the results without and with AAU loss, respectively.

TABLE VII
THE EVALUATION ON AU LOSS AND AAU LOSS. ACC(%).

| Models | Basic Model | | AU Loss | | AAU Loss | |
|------------------|-------------|-------|--------------|--------------|--------------|--------------|
| | ACC | F1 | ACC | F1 | ACC | F1 |
| GTS-GN (layer 1) | 72.91 | 0.697 | 73.31 | 0.728 | 75.70 | 0.749 |
| GTS-GN (layer 2) | 74.10 | 0.730 | 74.50 | 0.738 | 77.29 | 0.765 |
| GTS-GN (layer 3) | 74.90 | 0.720 | 75.30 | 0.745 | 75.30 | 0.744 |
| GTS-GN (layer 4) | 70.52 | 0.688 | 71.31 | 0.697 | - | - |

(a) On CAMSE II

| Models | Basic Model | | AU Loss | | AAU Loss | |
|------------------|-------------|-------|---------|-------|--------------|--------------|
| | ACC | F1 | ACC | F1 | ACC | F1 |
| GTS-GN (layer 1) | 70.92 | 0.673 | 75.18 | 0.743 | 77.30 | 0.765 |
| GTS-GN (layer 2) | 76.60 | 0.739 | 75.18 | 0.722 | 79.43 | 0.778 |
| GTS-GN (layer 3) | 73.76 | 0.700 | 77.30 | 0.767 | 78.72 | 0.782 |
| GTS-GN (layer 4) | 78.01 | 0.782 | 77.30 | 0.753 | - | - |

(b) On SAMM

still improves the performances of the model in most cases. The above results show that before the classification layer, the use of AU information to constraint features can improve the performance of MER. More detailed, although AU loss and AAU loss have similar performance for GTS-GN (layer 3) on CASME II, for all other cases, AAU loss is superior to AU loss, which demonstrates that it is more advantageous to adaptively constrain multi-scale features in multiple layers than fixedly constrain the features of a certain layer for MER.

Visualization: We further analyze AAU loss by showing the learned weight values $\frac{W_r^2}{\sum_{r=1}^{N_L} W_r^2}$ and visualizing the features in different layers. GTS-GN (layer 1) is taken as an example, so there are four learnable weights, namely $N_L = 4$. Table VIII shows the learned four weights for 26 subjects on CASME II,

and it turns out that the two weights for the first two layers are much larger than that for the last two layers, which shows that AAU loss focuses on limiting the features on the first two layers to aggregate AU information. In fact, the movements of landmarks have a direct relationship with AU, thus, AAU loss can constrain the feature to achieve the aggregation of high-level AU information on more early layers.

To verify above points, we further visualize the features in different layers. t-SNE [50] is employed to visualize these features to be a scatter plot, and the visualization results with and without AAU loss are shown in Fig. 7. Obviously, comparing with not using AAU loss, the extracted feature have some regularities on the first two layers after using AAU loss. Specifically, for the first layer, the features of the same categories not using AAU loss hardly appear cluster, while after using AAU loss, those begin to cluster; for the second layer, the clustering effect using AAU loss is better than that not using AAU loss, e.g. for category III, the features not using AAU loss are distributed on the whole plane, while those using AAU loss are mainly distributed on the left side. In addition, Fig. 7f shows that the features have some special intersection relationships that correspond to the relationships between AUs and MEs. In fact, a ME is related to single or multiple AUs, and different MEs may have a common AU, e.g. both II and V include AU1, and both III and IV include AU4, AU5 and AU7 (corresponding to Fig. 7f, the features of II and V or III and IV have some intersections). Above results demonstrate that AAU loss can constrain the features of the earlier layers to represent high-level AU information, which is consistent with the learned weights. Based on the AU-related features learned in the first two layers, AAU has obvious advantages for the features of the latter two layers. Specifically, for the third

TABLE VIII
THE LEARNED WEIGHTS FOR 26 SUBJECTS ON CASME II.

| layer | 1 | 2 | 3 | 4 |
|------------|--------|--------|--------|--------|
| Subject 1 | 0.5662 | 0.4127 | 0.0010 | 0.0201 |
| Subject 2 | 0.6992 | 0.2246 | 0.0118 | 0.0643 |
| Subject 3 | 0.6732 | 0.2727 | 0.0064 | 0.0477 |
| Subject 4 | 0.5312 | 0.4448 | 0.0055 | 0.0119 |
| Subject 5 | 0.6153 | 0.3296 | 0.0005 | 0.0546 |
| Subject 6 | 0.6404 | 0.3064 | 0.0003 | 0.0529 |
| Subject 7 | 0.6879 | 0.2514 | 0.0111 | 0.0497 |
| Subject 8 | 0.6078 | 0.3593 | 0.0000 | 0.0329 |
| Subject 9 | 0.6376 | 0.2848 | 0.0002 | 0.0774 |
| Subject 10 | 0.6724 | 0.2545 | 0.0025 | 0.0705 |
| Subject 11 | 0.6411 | 0.3087 | 0.0005 | 0.0498 |
| Subject 12 | 0.6625 | 0.2844 | 0.0033 | 0.0499 |
| Subject 13 | 0.6161 | 0.3341 | 0.0002 | 0.0495 |
| Subject 14 | 0.6056 | 0.3657 | 0.0000 | 0.0287 |
| Subject 15 | 0.6035 | 0.3484 | 0.0009 | 0.0417 |
| Subject 16 | 0.6801 | 0.2621 | 0.0080 | 0.0498 |
| Subject 17 | 0.5765 | 0.3853 | 0.0025 | 0.0357 |
| Subject 18 | 0.6387 | 0.3238 | 0.0017 | 0.0358 |
| Subject 19 | 0.6515 | 0.3021 | 0.0022 | 0.0441 |
| Subject 20 | 0.6758 | 0.2470 | 0.0027 | 0.0745 |
| Subject 21 | 0.5488 | 0.4267 | 0.0033 | 0.0211 |
| Subject 22 | 0.6039 | 0.3501 | 0.0007 | 0.0452 |
| Subject 23 | 0.6418 | 0.3126 | 0.0009 | 0.0446 |
| Subject 24 | 0.6341 | 0.3256 | 0.0007 | 0.0396 |
| Subject 25 | 0.6668 | 0.2760 | 0.0035 | 0.0537 |
| Subject 26 | 0.6781 | 0.2558 | 0.0050 | 0.0611 |
| Average | 0.6329 | 0.3172 | 0.0029 | 0.0464 |

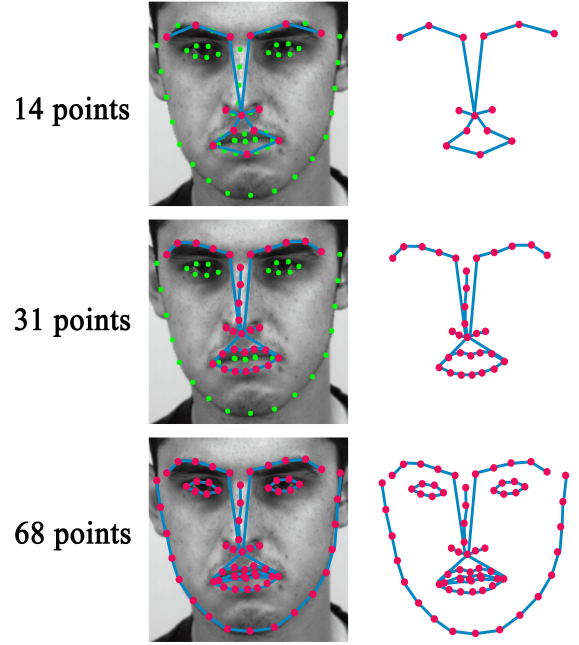


Fig. 8. Three types of point sets.

TABLE IX
THE EVALUATION ON THREE TYPES OF LANDMARK POINT SETS. ACC(%).

| Point number | CAMSE II | | SAMM | |
|--------------|----------|-------|-------|-------|
| | ACC | F1 | ACC | F1 |
| 14 | 72.91 | 0.716 | 75.17 | 0.732 |
| 31 | 72.91 | 0.693 | 72.34 | 0.691 |
| 68 | 72.50 | 0.704 | 68.79 | 0.608 |

layer as shown in Fig. 7c and 7g, the features using AAU loss obviously are superior to those not using AAU loss whether in terms of intra-class or inter-class; for the last layer, the features using AAU loss still maintain the advantage with larger inter-class and smaller intra-class. Overall, AAU loss makes the features of the earlier layers have some rules derived from AU information, and based on it, the features of the deeper layers are more discriminative to classify MEs.

D. Parameter Evaluation

In this section, the affect of the used landmark points and the trade-off parameter β are evaluated for the proposed method. We test three types of the landmark point sets as shown in Fig. 8, and β are tested to show the balance between AAU loss and ME loss.

The Affect of the Used Landmark Points:

Except for the 14 points of the graph defined in the 3.1 section, other two types of landmark point sets are tested, including 1) 31 points: all landmark points of mouth, nose and eyebrows regions; and 2) 68 points: all landmark points of whole face. Table IX shows the comparative results. Obvious, 14 points set has an obvious advantage and the performance of 68 points set is worst. It turns out that with the point number increases under including the key information of eyebrows, nodes, and mouth, the performance drops. In fact, compared

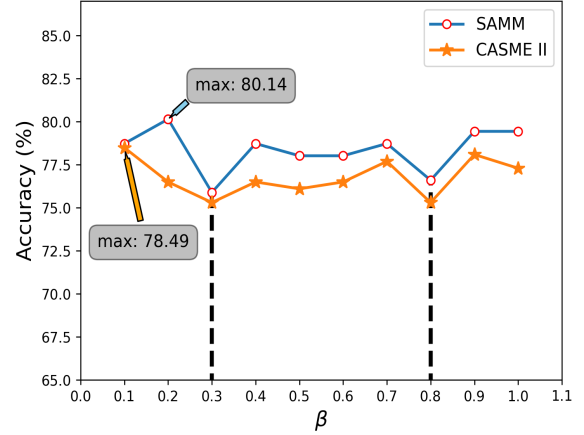


Fig. 9. The evaluation on β . The black dotted line represents the valley value.

with 14 points set, 31 points set includes redundant information, while 68 points set not only contains a lot of redundant information, but also some interference information, e.g. the eyes and facial contours. Also, 14 points set has fewer points, which reduces the computational cost and improves efficiency. Thus, removing interference points as well as redundant points and retaining key information for eyebrows, nose, and mouth is beneficial to improve performance and efficiency.

The Affect of β : Fig. 9 shows the results of the evaluation on β . The highest accuracy is achieved under $\beta=0.1$ (78.49%) on CAMSE II and $\beta=0.2$ (80.14%) on SAMM. Furthermore, under $\beta=0.3$ and 0.8, the performances on both datasets reach the valley. In general, the performance under β closing to 0.1 or 1 is superior to that under β in the middle value from 0.1 to 1. In detail, under β closing to 0.1, the highest accuracy can be achieved, which means that it is a better choice to take AU information as auxiliary information and remain the maintain dominance of ME loss.

TABLE X
COMPARING WITH OTHER METHODS UNDER 5 CATEGORIES BASED ON
AUS ANNOTATION. ACC(%).

| Methods | CAMSE II | | SAMM | |
|---------------------|--------------|--------------|--------------|--------------|
| | ACC | F1 | ACC | F1 |
| LBP-TOP [51] | 67.80 | 0.510 | 44.70 | 0.350 |
| HOOF [51] | 69.64 | 0.560 | 42.17 | 0.330 |
| HOG3D [51] | 69.53 | 0.510 | 34.16 | 0.220 |
| TL [46] | 75.68 | 0.650 | 70.59 | 0.540 |
| ELRCN-TE [52] | 52.44 | 0.500 | N/A | N/A |
| The proposed method | 87.21 | 0.848 | 72.06 | 0.709 |

E. Comparing with Other Methods

To evaluate the proposed method, we compare to some existing state-of-the-art methods. As shown in Table X, comparing with the existing methods recognizing five ME categories based on AU labels, GTS-GN provides a much better performance on both datasets and achieves new SOTA performances, especially, in terms of ACC and F1-score, 11.53% and 0.198 higher on CASME II and 1.47% and 0.169 higher on SAMM than TL that has SOTA performance.

For a more comprehensive comparison, we further test the results with five ME categories based on self-report labels, and it is also the mainstream test categories. According to Table XI, GTS-GN gets a comparable performance as a whole comparing with recent methods. Specifically, compared to the CNN-based methods, GEME and LGCcon, GTS-GN provides a much better performance on both datasets. Also, GACN and GRAUF are SOTA methods. Comparing with GRAUF, GTS-GN get a bit worse results on SAMM and a better results on CASME II, especially in terms of F1-score (0.107 higher than GRAUF on CASME II). Different from our method with a compact landmarks representation, GRAUF employed several models to extract features and also aggregated more information, *e.g.* AUs and magnified shape, which increases model complexity and reduces efficiency. Comparing with GACN, the proposed method also consistently shows obvious advantages on CASME II, but on SAMM, GACN get better performances. This maybe because that except geometric features of landmarks, GACN also utilized optical flow map for dynamic information, but it needs to spend much more computational cost to extract optical flow.

Overall, different from these existing methods, the compact landmarks input makes our model achieving a competitive performance with a lot less computational cost. All of these show the proposed method is effective and more suitable for practical applications.

V. CONCLUSION

This paper explored the connection of facial landmarks and graph model and demonstrated the effectiveness of landmarks for MER. Notably, only the geometric information of facial landmarks are aggregated by the GCN and TCN based graph model to achieve MER task. We first customized a GM-Graph based on the landmarks of three frames to model the geometric and dynamic information in ME videos. Then, SS module was proposed to learn the deep spatial and temporal features of GM-Graph. The experiments showed that SS module can aggregate the spatial and temporal information better,

TABLE XI
COMPARING WITH OTHER METHODS UNDER 5 CATEGORIES BASED ON
SELF-REPORT ANNOTATION. ACC(%).

| Methods | CAMSE II | | SAMM | |
|----------------------------|--------------|--------------|--------------|--------------|
| | ACC | F1 | ACC | F1 |
| Hierarchical LBP-IP [13] | 63.83 | 0.61 | N/A | N/A |
| Discriminative LBP-IP [28] | 64.78 | N/A | N/A | N/A |
| Sparse MDMO [11] | 66.95 | 0.691 | N/A | N/A |
| LBP-SDG [7] | 71.32 | 0.665 | N/A | N/A |
| KTGSL [15] | 72.58 | 0.682 | 56.11 | 0.493 |
| SSSN [34] | 71.19 | 0.715 | 56.62 | 0.451 |
| DSSN [34] | 70.78 | 0.729 | 57.35 | 0.464 |
| G-TCN [9] | 73.98 | 0.725 | 75.00 | 0.699 |
| GEME [33] | 75.20 | 0.735 | 55.88 | 0.454 |
| LGCcon [14] | 65.02 | 0.640 | 40.90 | 0.340 |
| GRAUF [22] | 74.27 | 0.705 | 74.26 | 0.705 |
| GACN [10] | 81.30 | 0.709 | 88.24 | 0.828 |
| The proposed method | 81.78 | 0.812 | 71.32 | 0.711 |

namely, it's more suitable to introduce both GCN and TCN to separately aggregate the spatial and temporal information. To further improve the performance, geometric information including the low-order coordinates and high-order semantic features are both involved. Therefore, a new graph model GTS-GN, which models information interaction and takes better use of complementary information from two types of geometric features, was proposed. Furthermore, the proposed LAM can automatically learn a more reasonable graph structure that builds the relationship between different facial muscle regions and between different nodes. In addition, the proposed AAU loss can consider the strong correlations of AUs and MEs and constrain the features in a multi-scale fashion to aggregate AU information for adaptively learning more discriminative ME features.

This work encourages further investigation of low-dimensional landmarks as input with graph-based model to extract compact geometric features, which is more valuable for practical applications due to its low computational costs and at the same time comparable and even superior performance.

ACKNOWLEDGMENT

This work was partly supported by the Postgraduate Research and Practice Innovation Program of Jiangsu Province (Grant KYCX18_0899), partly by the National Natural Science Foundation of China (NSFC) under Grants 72074038, partly by the National Natural Science Foundation of China (NSFC) (Grants 61971236).

REFERENCES

- [1] S. Porter and L. Brinke, "Reading between the lies," *Psychological science*, vol. 19, pp. 508–14, 06 2008.
- [2] P. Ekman, *Telling lies clues to deceit in the marketplace, politics, and marriage*, 1991.
- [3] P. Ekman, *Lie Catching and Microexpressions*. The Philosophy of Deception, 07 2009.
- [4] S. Weinberger, "Airport security: Intent to deceive?" *Nature*, vol. 465, pp. 412–5, 05 2010.
- [5] W. Yan, Q. Wu, Y. Chen, J. Liang, and X. Fu, "How fast are the leaked facial expressions: The duration of micro-expressions," *Journal of Nonverbal Behavior*, vol. 37, 12 2013.
- [6] Z. Xia, W. Peng, H.-Q. Khor, X. Feng, and G. Zhao, "Revealing the invisible with model and data shrinking for composite-database micro-expression recognition," *IEEE Transactions on Image Processing*, vol. 29, pp. 8590–8605, 2020.

- [7] J. Wei, G. Lu, and J. Yan, "A comparative study on movement feature in different directions for micro-expression recognition," *Neurocomputing*, vol. 449, pp. 159–171, 2021.
- [8] N. V. Quang, J. Chun, and T. Tokuyama, "CapsuleNet for micro-expression recognition," in *2019 14th IEEE International Conference on Automatic Face Gesture Recognition (FG 2019)*, 2019, pp. 1–7.
- [9] L. Lei, J. Li, T. Chen, and S. Li, "A novel graph-tcn with a graph structured representation for micro-expression recognition," in *Proceedings of the 28th ACM International Conference on Multimedia*, ser. MM '20. New York, NY, USA: Association for Computing Machinery, 2020, p. 2237–2245.
- [10] A. J. R. Kumar and B. Bhanu, "Micro-expression classification based on landmark relations with graph attention convolutional network," in *Proceedings of the IEEE/CVF Conference on Computer Vision and Pattern Recognition (CVPR) Workshops*, June 2021, pp. 1511–1520.
- [11] Y.-J. Liu, B.-J. Li, and Y.-K. Lai, "Sparse mdmo: Learning a discriminative feature for spontaneous micro-expression recognition," *IEEE Transactions on Affective Computing*, vol. PP, pp. 1–1, 07 2018.
- [12] B. Song, K. Li, Y. Zong, J. Zhu, W. Zheng, J. Shi, and L. Zhao, "Recognizing spontaneous micro-expression using a three-stream convolutional neural network," *IEEE Access*, vol. 7, pp. 184 537–184 551, 2019.
- [13] Y. Zong, X. Huang, W. Zheng, Z. Cui, and G. Zhao, "Learning from hierarchical spatiotemporal descriptors for micro-expression recognition," *IEEE Transactions on Multimedia*, vol. 20, pp. 3160–3172, 11 2018.
- [14] Y. Li, X. Huang, and G. Zhao, "Joint local and global information learning with single apex frame detection for micro-expression recognition," *IEEE Transactions on Image Processing*, vol. 30, pp. 249–263, 01 2021.
- [15] J. Wei, G. Lu, J. Yan, and Y. Zong, "Learning two groups of discriminative features for micro-expression recognition," *Neurocomputing*, vol. 479, pp. 22–36, 2022.
- [16] W. Peng, X. Hong, Y. Xu, and G. Zhao, "A boost in revealing subtle facial expressions: A consolidated eulerian framework," in *14th IEEE International Conference on Automatic Face and Gesture Recognition (FG 2019)*, 2019.
- [17] H.-X. Xie, L. Lo, H.-H. Shuai, and W.-H. Cheng, "Au-assisted graph attention convolutional network for micro-expression recognition," in *Proceedings of the 28th ACM International Conference on Multimedia*, ser. MM '20. New York, NY, USA: Association for Computing Machinery, 2020, p. 2871–2880.
- [18] G. Zhao and M. Pietikainen, "Dynamic texture recognition using local binary patterns with an application to facial expressions," *IEEE Transactions on Pattern Analysis and Machine Intelligence*, vol. 29, no. 6, pp. 915–928, June 2007.
- [19] J. Wei, G. Lu, J. Yan, and H. Liu, "Micro-expression recognition using local binary pattern from five intersecting planes," *Multimedia Tools and Applications*, 2022.
- [20] Y.-H. Oh, J. See, A. C. Le Ngo, R. C.-W. Phan, and V. M. Baskaran, "A survey of automatic facial micro-expression analysis: Databases, methods, and challenges," *Frontiers in psychology*, vol. 9, p. 1128, 2018.
- [21] D. Y. Choi and B. C. Song, "Facial micro-expression recognition using two-dimensional landmark feature maps," *IEEE Access*, vol. 8, pp. 121 549–121 563, 2020.
- [22] L. Lei, T. Chen, S. Li, and J. Li, "Micro-expression recognition based on facial graph representation learning and facial action unit fusion," in *Proceedings of the IEEE/CVF Conference on Computer Vision and Pattern Recognition (CVPR) Workshops*, June 2021, pp. 1571–1580.
- [23] L. Zhou, Q. Mao, and M. Dong, "Objective class-based micro-expression recognition through simultaneous action unit detection and feature aggregation," *ArXiv*, vol. abs/2012.13148, 2020.
- [24] L. Lo, H.-X. Xie, H.-H. Shuai, and W.-H. Cheng, "Mer-gcn: Micro-expression recognition based on relation modeling with graph convolutional networks," in *2020 IEEE Conference on Multimedia Information Processing and Retrieval (MIPR)*, 2020, pp. 79–84.
- [25] P. Ekman and W. Friesen, "Facial action coding system: A technique for the measurement of facial movement," *Consulting Psychologists Press Palo Alto*, vol. 12, 01 1978.
- [26] X. Li, T. Pfister, X. Huang, G. Zhao, and M. Pietikainen, "A spontaneous micro-expression database: Inducement, collection and baseline," in *2013 10th IEEE International Conference and Workshops on Automatic Face and Gesture Recognition, FG 2013*, 04 2013, pp. 1–6.
- [27] S.-T. Liong, R. Phan, J. See, Y.-H. Oh, and K. Wong, "Optical strain based recognition of subtle emotions," in *2014 International Symposium on Intelligent Signal Processing and Communication Systems (ISPACS)*, 01 2015, pp. 180–184.
- [28] X. Huang, S. Wang, X. Liu, G. Zhao, X. Feng, and M. Pietikäinen, "Discriminative spatiotemporal local binary pattern with revisited integral projection for spontaneous facial micro-expression recognition," *IEEE Transactions on Affective Computing*, vol. 10, no. 1, pp. 32–47, Jan 2019.
- [29] F. Xu, J. Zhang, and J. Wang, "Microexpression identification and categorization using a facial dynamics map," *IEEE Transactions on Affective Computing*, vol. 8, pp. 254–267, 2017.
- [30] Y.-J. Liu, J.-K. Zhang, W.-J. Yan, S.-J. Wang, G. Zhao, and X. Fu, "A main directional mean optical flow feature for spontaneous micro-expression recognition," *IEEE Transactions on Affective Computing*, vol. 7, no. 4, pp. 299–310, 2016.
- [31] S. Polikovskiy, Y. Kameda, and Y. Ohta, "Facial micro-expressions recognition using high speed camera and 3d-gradient descriptor," in *3rd International Conference on Imaging for Crime Detection and Prevention (ICDP 2009)*, 01 2010, pp. 1 – 6.
- [32] X. Li, X. Hong, A. Moilanen, X. Huang, T. Pfister, G. Zhao, and M. Pietikäinen, "Towards reading hidden emotions: A comparative study of spontaneous micro-expression spotting and recognition methods," *IEEE Transactions on Affective Computing*, vol. 9, no. 4, pp. 563–577, 2018.
- [33] X. Nie, M. A. Takalkar, M. Duan, H. Zhang, and M. Xu, "Geme: Dual-stream multi-task gender-based micro-expression recognition," *Neurocomputing*, vol. 427, pp. 13–28, 2021.
- [34] H.-Q. Khor, J. See, S. Liong, R. Phan, and W. Lin, "Dual-stream shallow networks for facial micro-expression recognition," in *2019 IEEE International Conference on Image Processing*, 09 2019, pp. 36–40.
- [35] M. Verma, S. K. Vipparthi, G. Singh, and S. Murala, "Learnnet: Dynamic imaging network for micro expression recognition," *IEEE Transactions on Image Processing*, vol. 29, pp. 1618–1627, 2020.
- [36] S. Liong, J. See, R. Phan, K. Wong, and S.-W. Tan, "Hybrid facial regions extraction for micro-expression recognition system," *Journal of Signal Processing Systems*, vol. 90, 04 2018.
- [37] L. Zhong, C. Bai, J. Li, T. Chen, S. Li, and Y. Liu, "A graph-structured representation with brnn for static-based facial expression recognition," in *2019 14th IEEE International Conference on Automatic Face Gesture Recognition (FG 2019)*, 2019, pp. 1–5.
- [38] T. Kipf and M. Welling, "Semi-supervised classification with graph convolutional networks," in *Conference Track Proceedings of the 2017 International Conference on Learning Representations (ICLR)*, 2017.
- [39] S. Bai, J. Z. Kolter, and V. Koltun, "An empirical evaluation of generic convolutional and recurrent networks for sequence modeling," 2018.
- [40] S. Yan, Y. Xiong, and D. Lin, "Spatial temporal graph convolutional networks for skeleton-based action recognition," *Proceedings of the AAAI Conference on Artificial Intelligence*, vol. 32, no. 1, Apr. 2018.
- [41] T.-K. Tran, Q.-N. Vo, X. Hong, X. Li, and G. Zhao, "Micro-expression spotting: A new benchmark," *Neurocomputing*, vol. 443, pp. 356–368, 2021.
- [42] S.-J. Wang, Y. He, J. Li, and X. Fu, "Mesnet: A convolutional neural network for spotting multi-scale micro-expression intervals in long videos," *IEEE Transactions on Image Processing*, vol. 30, pp. 3956–3969, 2021.
- [43] A. Paszke, S. Gross, F. Massa, A. Lerer, J. Bradbury, G. Chanan, T. Killeen, Z. Lin, N. Gimelshein, L. Antiga, A. Desmaison, A. Köpf, E. Yang, Z. DeVito, M. Raison, A. Tejani, S. Chilamkurthy, B. Steiner, L. Fang, J. Bai, and S. Chintala, "Pytorch: An imperative style, high-performance deep learning library," 2019.
- [44] A. Davison, C. Lansley, N. Costen, K. Tan, and M. H. Yap, "Samm: A spontaneous micro-facial movement dataset," *IEEE Transactions on Affective Computing*, vol. 9, no. 1, pp. 116–129, 2018.
- [45] W. Yan, X. Li, S. Wang, G. Zhao, Y. Liu, Y. Chen, and X. Fu, "Casmee ii: An improved spontaneous micro-expression database and the baseline evaluation," *PLOS ONE*, vol. 9, no. 1, pp. 1–8, 2014.
- [46] M. Peng, Z. Wu, Z. Zhang, and T. Chen, "From macro to micro expression recognition: Deep learning on small datasets using transfer learning," in *2018 13th IEEE International Conference on Automatic Face Gesture Recognition (FG 2018)*, 2018, pp. 657–661.
- [47] T.-H. Oh, R. Jaroensri, C. Kim, M. Elgharib, F. Durand, W. T. Freeman, and W. Matusik, "Learning-based video motion magnification," in *Proceedings of the European Conference on Computer Vision*, Sep 2018.
- [48] V. Kazemi and J. Sullivan, "One millisecond face alignment with an ensemble of regression trees," in *Proceedings of the IEEE Conference on Computer Vision and Pattern Recognition (CVPR)*, June 2014.
- [49] J. Wan, Z. Lai, J. Li, J. Zhou, and C. Gao, "Robust facial landmark detection by multiorder multiconstraint deep networks," *IEEE Transactions on Neural Networks and Learning Systems*, pp. 1–14, 01 2021.
- [50] L. van der Maaten and G. Hinton, "Visualizing data using t-sne," *Journal of Machine Learning Research*, vol. 9, pp. 2579–2605, 11 2008.
- [51] A. Davison, W. Merghani, and M. H. Yap, "Objective classes for micro-facial expression recognition," *Journal of Imaging*, vol. 4, 08 2017.

- [52] H.-Q. Khor, J. See, R. C. W. Phan, and W. Lin, "Enriched long-term recurrent convolutional network for facial micro-expression recognition," in *2018 13th IEEE International Conference on Automatic Face Gesture Recognition (FG 2018)*, 2018, pp. 667–674.